Evaluation of a Regional Atmospheric Model Using Measurements of Surface Heat Exchange Processes from a Site in Antarctica

NICOLE P. M. VAN LIPZIG

Royal Netherlands Meteorological Institute, de Bilt, the Netherlands, and Institute for Marine and Atmospheric Research Utrecht, Utrecht, the Netherlands

ERIK VAN MEIJGAARD

Royal Netherlands Meteorological Institute, de Bilt, the Netherlands

JOHANNES OERLEMANS

Institute for Marine and Atmospheric Research Utrecht, Utrecht, the Netherlands

(Manuscript received 9 February 1998, in final form 28 August 1998)

ABSTRACT

A regional atmospheric climate model with a horizontal grid spacing of 55 km has been used to simulate the Antarctic atmosphere during an austral summer period. ECMWF reanalyses were used to force the atmospheric prognostic variables from the lateral boundaries. Sea surface temperatures and the sea ice mask in the model were prescribed from observations. Parameterizations of the physical processes were taken from the ECHAM4 general circulation model. Before applying the model to Antarctic conditions, several adjustments had been made to the original code. In particular, a better correspondence between model output and measurements was accomplished by 1) the use of a fixed value of 0.8 for the surface albedo rather than applying an albedo that linearly rises with surface temperature and 2) the use of the volumetric heat capacity and the thermal diffusivity of snow rather than employing the values for ice.

The model is evaluated for the period 14–19 January 1993 (P1) on the basis of an extensive dataset compiled from measurements made at a site (Svea) in Dronning Maud Land. This dataset contains boundary layer temperature and specific humidity profiles, snow temperatures, and surface heat fluxes. The surface fluxes were obtained from direct measurements combined with an energy balance model. The atmospheric temperature profiles simulated at the grid points corresponding most closely to Svea are in good agreement with the measured profiles, although the model slightly overestimates the vertical temperature gradient. The model probably underestimates the turbulent transport of heat and moisture to atmospheric layers above roughly 200 m. At Svea a cloud cover of less than 0.5 octas was observed during P1. The model overestimates the cloud cover, which results in an underestimation of shortwave and an overestimation of longwave radiative fluxes at the surface. The simulated values for the net radiative fluxes, the heat flux into the snow, and the turbulent heat fluxes correspond within 4 W m^{-2} to the fluxes that were inferred from measurements.

1. Introduction

The evaluation of large-scale atmospheric models is limited mainly to data-rich areas. It is not clear in advance that current atmospheric models are suitable for simulating the climate of Antarctica. Application of the model to the extreme meteorological conditions present on the ice cap is a severe test for the parameterization of the physical processes. Despite the progress in recent years, parameterizations used in general circulation models (GCMs) still show inadequacies when used in simulations of atmospheric processes in polar regions (e.g., Tzeng et al. 1994; Genthon 1994; Connolley and Cattle 1994; King and Connolley 1997; Krinner et al. 1997). It is important to study the ability of large-scale models to simulate the atmospheric conditions in Antarctica. Among others, these models are important tools for studying the interaction between large-scale circulation and surface exchange processes. Knowledge of this interaction is a prerequisite to explain information from ice cores in terms of the natural variations in the past climate. In addition, studying the ability of the parameterizations to simulate the physical processes in extreme conditions helps to identify deficiencies in these parameterizations that can be useful to improve atmospheric models, not only for Antarctica but also for other regions of the world.

Corresponding author address: Dr. Nicole P. M. van Lipzig, KNMI, P.O. Box 201, 3730 AE de Bilt, the Netherlands.
E-mail: lipzig@knmi.nl

Simulations of the atmosphere over Antarctic regions with limited area models (LAMs) nested in European Centre for Medium-Range Weather Forecasts (ECMWF) analyses have been performed with various objectives. Hines et al. (1995) employed a cloud-free version of the National Center for Atmospheric Research Mesoscale Model version 4. They found that the model is able to simulate realistic synoptic phenomena although the lack of latent heating results in some biases. The results of a comparison with automatic weather station data suggest that the model has a typical cold bias of about 2°C for June 1988. The addition of moist physics to the model tends to improve the quality of the fields over the southern oceans, but excessively high temperatures at the surface and higher up in the troposphere are found due to an overestimation of atmospheric back radiation by clouds (Hines et al. 1997). Walsh and McGregor (1996) performed July simulations with the Division of Atmospheric Research Limited Area Model (DARLAM) and found that the surface air temperatures in the interior of the continent are mainly higher in DARLAM than in the ECMWF analyses. DARLAM represents the average July accumulated snowfall rather well with a slight tendency to overestimate it in regions of steep orography and in parts of the interior. A $\Delta x = 25$ km model nested in a $\Delta x = 50$ km LAM was used to study mesocyclones in the Weddell Sea (Engels and Heinemann 1996) and to study the katabatic wind in the same area (Heinemann 1997). A detailed comparison between model output and measurements is one of the goals of the Antarctic First Regional Observing Study of the Troposphere (FROST) project (Turner et al. 1996). Data obtained within this project will be very valuable for model evaluation. The FROST project focuses on operational analyses and forecasts for the Antarctic continent and the surrounding ocean areas.

Sparcity of data hampers model evaluation for the Antarctic ice cap. Most previous sites where measurements are performed are located near the coast. Besides, evaluation of atmospheric models for Antarctica is often confined to a comparison between model output and surface values. However, in this study boundary layer profiles of temperature and humidity, surface heat fluxes, and temperatures in the snow measured at a station located between the interior and the coast are used. These data were obtained from an extensive field campaign performed by the Institute for Marine and Atmospheric Research, Utrecht (IMAU), during the period December 1992–February 1993 at the Swedish station Svea (74°35′S, 11°13′W). Svea is located in Dronning Maud Land at a distance of 290 km from the coast. A combination of meteorological data is necessary to test whether the physical parameterizations are able to simulate the processes in the Antarctic atmosphere properly.

The model used in this study is the regional model HIRHAM (HIRLAM–ECHAM)/Regional Atmospheric Climate Model (RACMO; Christensen et al. 1996), hereafter referred to as RACMO. In this model, the parameterizations of the physical processes are taken from the ECHAM4 GCM, which is used at the Max-Planck-Institut für Meteorologie in Hamburg (Roeckner et al. 1996), with a few adjustments being made to the original code. The snow albedo parameterization, the characteristics of snow, the initialization of the temperature in the snow, and the roughness length are adapted. An extra vertical layer is inserted at a height of 8 m. The model is operational at a horizontal grid spacing of 55 km. This resolution is comparable to the current operational resolution (T319) of the global ECMWF model, which is equivalent to a horizontal grid spacing of about 63 km. A resolution in the order of 50 km is needed to resolve the steep edges of the Antarctic ice cap with roughly 10 points. An earlier study showed that the model is capable of simulating realistic profiles of temperature and humidity at South Polar station and Georg-von-Neumayer (van Lipzig et al. 1998). Simulations with RACMO have also been performed for other regions of the world. The model was evaluated before by Christensen et al. (1997) for climate simulations over Europe. They found large improvements after the ECHAM3 physical parameterizations had been replaced by the ECHAM4 parameterizations. Dethloff et al. (1996) used the model, with ECHAM3 physics, to simulate the climate of the Arctic region and found that the model reproduces the ECMWF-analyzed monthly mean circulation rather closely. They also found that the model underestimates vertical transports of heat and moisture in the planetary boundary layer in wintertime.

The operational ECMWF analyses are widely used for studying the climate of Antarctica (e.g., Bromwich et al. 1995; Budd et al. 1995; Genthon and Braun 1995). They have been verified in Antarctic latitudes within the framework of the FROST project by Cullather et al. (1997). Operational analyses are known to have problems in simulating boundary layer processes in stable conditions (Beljaars 1995). The ECMWF reanalyses (ERA) were constructed in order to obtain a consistent set of analyses that can be used for climate studies. They were composed by reassimilating data for the period from 1979 to 1994 into a simulation with the ECMWF model at T106 resolution and 31 atmospheric vertical layers (Gibson et al. 1997). The IMAU measurements are very useful to evaluate the ECMWF reanalyses since they were not used in the assimilation procedure.

The objective of this paper is to compare model output of RACMO with boundary layer profiles of temperature and humidity, snow temperatures, and surface heat fluxes measured at the Swedish research station Svea. It is interesting to see whether the use of a boundary layer scheme different than the scheme that was used in the ERA project has a large impact on the model performance in stable conditions. In the future, spatially detailed information on the temperature distribution in the Antarctic region and the surface mass balance on the ice cap will be obtained from longer integrations.

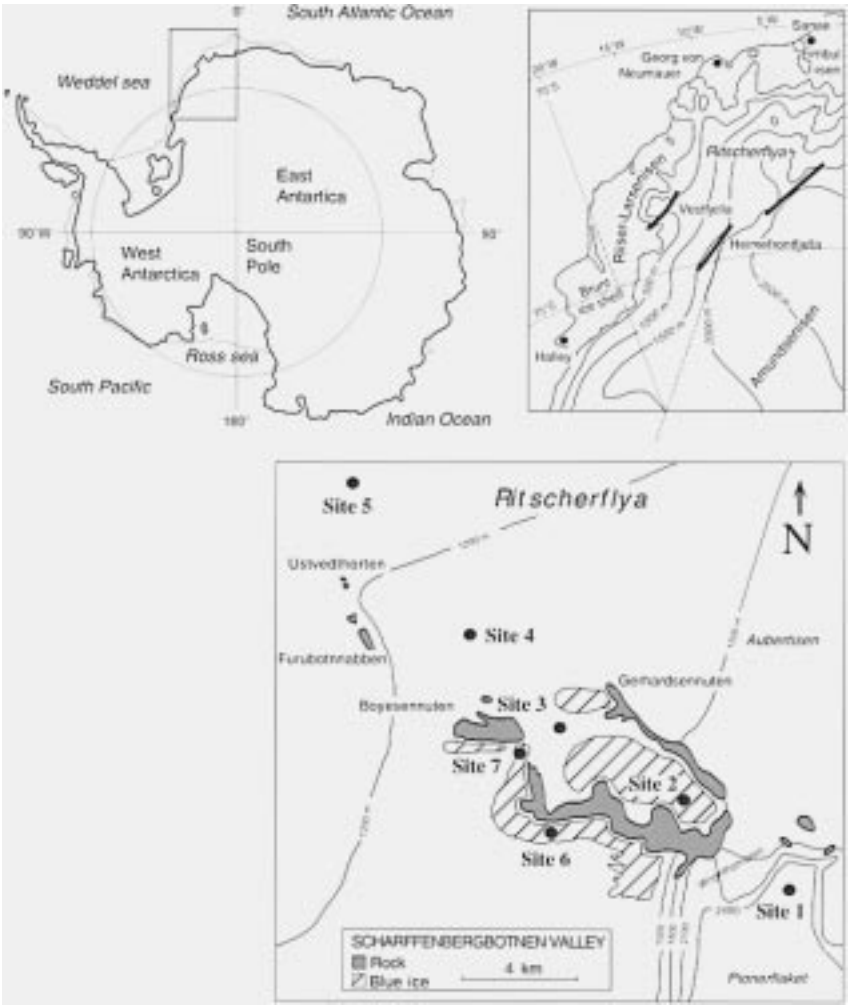

FIG. 1. Map of the location of Scharffenbergbotnen, Heimefrontfjella, Dronning Maud Land, East Antarctica (adopted from Bintanja and van den Broeke 1995). The upper panel on the right shows the surroundings of the Heimefrontfjella. The lower panel show the Scharffenbergbotnen Valley with some topographic detail. Measurements were performed at the seven sites indicated in this panel. The research station Svea is located at site 7.

In addition, the sensitivity of the mass balance to climatic perturbations will be studied. In this paper, model output from a simulation of the 14-day period 6–19 January 1993 is compared with the measurements performed near Svea. Sections 2 and 3 briefly describe the measurements and the model setup. In section 4 we present a comparison of model output with measurements of temperature and humidity profiles, and surface fluxes at Svea. The ECMWF reanalyses are also discussed in this section. The impact of the adjustments to the original code is discussed in section 5. A summary is given in section 6.

2. Measurements at Svea

In the austral summer of 1992–93, detailed boundary layer and surface flux measurements were performed at the Swedish research station Svea (74°35′S, 11°13′W) in Dronning Maud Land (Bintanja et al. 1993). Svea is situated near a U-shaped valley called Scharffenbergbotnen in the central part of the Heimefront Range at an elevation of 1250 m above sea level and at a distance of 290 km from the coast (Fig. 1).

Temperature and wind speed measurements at heights of 2 and 6 m were performed at seven sites in and around the valley. The sites are indicated in Fig. 1. In addition, relative humidity was measured at heights of 2 and 6 m, at sites 2, 3, and 7. Shortwave up- and downward and total up- and downward radiative fluxes were measured at sites 2 and 3. Bintanja and van den Broeke (1995) used an energy balance model to derive surface fluxes from the measured quantities. We will refer to these fluxes as inferred fluxes throughout the paper. An estimate was made for the humidity at the sites where

this quantity was not measured. The uncertainty in inferred fluxes due to measuring inaccuracies are small (<1.2 W m^{-2}) compared to uncertainties due to assumptions made. The result is very sensitive to the employed value of the roughness length. Sites 4 and 5 were operational in the relatively undisturbed plateau regime and might be considered representative for a larger area corresponding to a model grid box. After all, the local circulation in the Scharffenbergbotnen Valley is not resolved by the model. Unfortunately, site 5 was not operational for the entire period, so the measurements from site 4 are used for the comparison with model output. From Fig. 1 it can be seen that blue ice areas are present in the surroundings of Svea. Measurements at site 2 were made above ice and therefore we used the radiative fluxes at site 3, which were made above snow.

In Fig. 2a, the mean daily cycle of surface radiative fluxes at site 3 is shown for the period 14–19 January 1993. Local noon is at 1237 UTC and at that time of the year the sun is above the horizon for 24 h per day. Most incoming shortwave radiation is reflected upward due to the high albedo (0.8) of the surface. The mean maximum surface temperature is observed between 1300 and 1400 UTC, so the outgoing longwave radiation is greatest at this time of the day. The daily variation of the incoming longwave radiation is small. Altogether, the net radiation is positive between roughly 0500 and 1700 UTC and negative for the remaining part of the day. The heat flux into the snow and the turbulent heat fluxes as derived from measurements at site 4 are shown in Fig. 2b. During the period of outgoing net radiation, the atmosphere becomes stably stratified resulting in a downward directed sensible heat flux. During the period of incoming net radiation, evaporation dominates the turbulent heat exchange at the surface. The sum of the radiative and turbulent fluxes is available for heating or cooling of the snow layers.

A helium-filled cable balloon was launched at site 7 every 3–6 h, provided the surface wind speed was less than 10 m s^{-1}. Pressure, temperature, humidity, and wind speed and direction were measured in the lowest 800 m of the boundary layer (van den Broeke and Bintanja 1995). Under conditions of outgoing net radiation at the surface, a stable boundary layer develops. The surface flow decouples from the upper air flow, resulting in an increase of specific humidity in the lowest 100 m of the atmosphere. At 0600 UTC the inversion strength is typically 7 K. When the boundary layer becomes neutral, specific humidity in the surface layer decreases and evaporation at the surface is enhanced. At 1500 UTC, the inversion strength is less than 1 K. The local climate inside of the valley is somewhat warmer and drier than the climate outside of this valley. Bintanja and van den Broeke (1995) compared data from sites 2 and 3 inside the valley to data from site 5 outside the valley and found that the temperature outside the valley is 1.6°C lower than the temperature at site 2 and 3.1°C lower than the temperature at site 3. On the basis of measurements from automatic weather stations, Jonsson (1992) concluded that the local climate in the valley near the surface is 0.2 g kg^{-1} drier than the climate in the undisturbed region.

For the comparison study, we use surface fluxes and atmospheric profiles of temperature and humidity as measured in the period 14–19 January 1993, which was a spell with fair weather. Also the measured temperature profiles in the snow are included. The area around site 7, where the cable balloon was launched, is characterized by rock outcrop and small valleys. Therefore the measured wind speed and direction cannot be considered to be representative for a grid box mean area of 55×55 km^2. For this reason, we have not included a comparison between measured and modeled wind speed and direction for the entire boundary layer. It is, however, important to remark that the differences in wind speed between model and measurements vanish at the model layer that is centered at 700 m. At this layer, the measured wind speed is 3.7 m s^{-1} and the simulated wind speed is 3.8 m s^{-1}. This result suggests that the model is able to properly simulate the wind speed that is representative of the free atmosphere at Svea.

3. The model

The horizontal model grid of RACMO is shown in Fig. 3a. It covers an area of 4.6×10^7 km^2, including the Antarctic continent and a large part of the Southern Ocean, with 122×130 grid points. In Fig. 3b the height of the surface is shown along a cross section as indicated by the black line in Fig. 3a. The steep gradients in the coastal zone of the continent are resolved with roughly 10 grid points. In the vertical, 20 hybrid layers (σ coordinates near the surface transforming gradually into nearly pressure coordinates in the stratosphere) are employed with the lowest layers centered at 8, 38, 139, 367, and 752 m. In the standard version of the model, the 8-m layer is not present. This layer close to the surface is inserted to obtain higher resolution in the generally shallow boundary layer of the Antarctic atmosphere.

The dynamical part of the model is taken from the numerical weather prediction model HIRLAM (High-Resolution Limited Area Model; Gustafsson 1993). In the lateral boundary zone of the model domain (larger dots in Fig. 3a) the prognostic variables are relaxed towards the output of a larger-scale model using a technique proposed by Dickinson et al. (1989). A time step of 4 min is used. The parameterizations of the physical processes are taken from the ECHAM4 GCM and a brief description of the various parameterizations is presented in Table 1.

ECMWF reanalyses are used to force the model at the lateral boundaries. The reanalyses were constructed by reassimilating data for the period from 1979 to 1994 into a simulation with the ECMWF model at T106 resolution (Gibson et al. 1997). The reanalyses are avail-

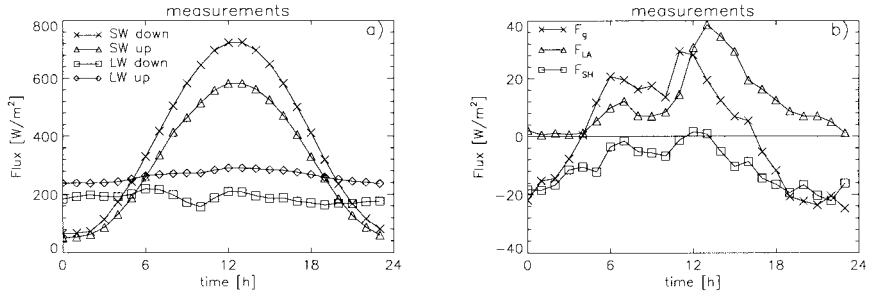

FIG. 2. Measured and inferred fluxes at (a) site 3 and (b) site 4, averaged over the period 14–19 Jan 1993 (P1). The shortwave flux is indicated by SW, the longwave flux is indicated by LW, F_G is the downward heat flux into the snow, F_{LA} is the upward latent heat flux, and F_{SH} is the upward sensible heat flux.

able every 6 h. Values at the lateral boundaries at intermediate times are obtained by linear interpolation. Sea surface temperature and the sea ice mask are prescribed from observations. The same values as employed in the ECMWF reanalyses are used. The fields are updated every 6 h. The sea ice mask is based on Special Sensor Microwave/Imager satellite measurements (Nomura 1995). A model grid box is either ice free or uniformly covered with sea ice of a constant thickness. The sea ice temperature is a prognostic variable, calculated from the surface energy budget and the upward heat flux from the ocean.

The model surface geopotential height (Z_{srf}) is prescribed by the Drewry topography (Drewry 1983). In Fig. 4a the location of the model grid points and the corresponding Z_{srf} are given. The surface elevation of the model grid point is representative for an area of 55 $\times$ 55 km^2 while the measurements are performed at a specific point. At the grid point closest to Svea Z_{srf} is 1510 m, which is 270 m higher than Z_{srf} at Svea. Model output of grid point g_2, with Z_{srf} 1230 m, is also analyzed. The ECMWF reanalyses were obtained from the archive of ECMWF on a regular latitude–longitude grid represented in Fig. 4b. In the ECMWF model, Z_{srf} is prescribed by the U.S. Navy dataset, which is known to be erroneous, especially in Dronning Maud Land (Genthon and Braun 1995). The height Z_{srf} of the ECMWF grid point m_4 (1180 m) is closest to the Z_{srf} value at Svea. RACMO uses the effective roughness length of the ECMWF model, maximized at 3 m.

Before applying the model to Antarctica, a few adjustments have been made to the parameterization of the albedo, the heat capacity, and the diffusivity of the snow layers and the snow temperature initialization. These adjustments are described briefly below.

a. Albedo

In the original code, the albedo (α) remains constant at a value of 0.80 for surface temperatures (T_s) below -10°C and is a prescribed function of temperature for surface temperatures above -10°C:

$$\alpha = 0.60 - 0.02T_s, \tag{1}$$

where T_s is given in degrees Celsius. For surface temperatures near the freezing point, this relation provides a rather low value for the albedo, which is not supported by observations. Measurements show that the albedo is in the range of 0.80 to 0.90 quite uniformly across the plateau (King and Turner 1997). Furthermore, the prescribed function leads to a positive feedback mechanism when the surface temperature increases. To prevent such an effect from happening, we have set the value of the albedo at 0.80 for all surface temperatures below the freezing point.

b. Characteristics of snow and ice

The subsurface temperature is determined using a five-layer model until a depth of 10 m. The heat flux (F) between the layers is calculated from

$$F = \rho C_g \kappa \frac{\partial T}{\partial z}, \tag{2}$$

where ρC_g is the heat capacity of the snow/ice per unit volume, κ the heat diffusivity, T the temperature, and z the vertical coordinate. The temperature tendency in a layer is calculated from the flux divergence over that layer:

$$\frac{\partial T}{\partial t} = \frac{1}{\rho C_g}\frac{\partial F}{\partial z}. \tag{3}$$

To establish the value of κ, we use the Mellor formula (Mellor 1977), which gives an estimate of κ as a function of ρ. Strictly speaking, ρ is a function of depth; however, for simplicity we assumed a constant and horizontally uniform value of 400 kg m^{-3}. This yields a value of 6.06×10^{-7} m^2 s^{-1} for κ, and 0.804×10^6 J m^{-3} K^{-1} for ρC_g.

In the original ECHAM code, the characteristics of ice are used to determine κ and ρC_g ($\kappa = 12 \times 10^{-7}$ m^2 s^{-1} and $\rho C_g = 2.09 \times 10^6$ J m^{-3} K^{-1}). However, the uppermost 10 m of the ice sheet consist mostly of snow because the metamorphosis from snow to ice is a

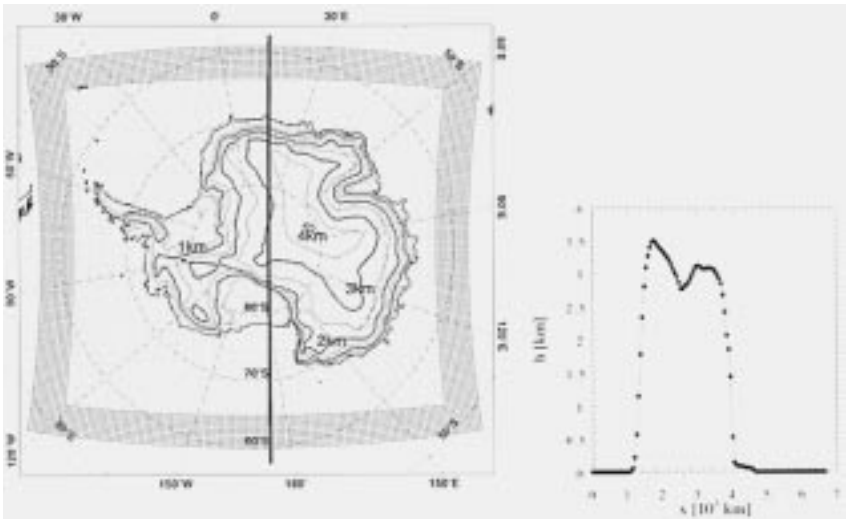

FIG. 3. (a) RACMO grid with a horizontal spacing of 55 km. In the relaxation zone (indicated by larger dots), the model prognostic variables are relaxed toward ECMWF reanalyses. The surface geopotential height (km) is indicated by the contour lines. (b) Model orography along the cross section indicated by the black line in (a). Dots refer to model grid points.

slow process in Antarctica due to the low temperatures (Herron and Langway 1980).

c. Initialization of the temperature profile in the snow

For relatively short model runs, less than a year, it is essential to initialize the snow temperatures with fairly realistic profiles. The snow temperature profile at a certain time of the year can be calculated from Eqs. (2) and (3), imposing an annual cycle on the surface temperature. A climatology of 12 monthly mean surface temperatures is prescribed for every grid point. We used a Fourier decomposition of the climatological annual cycle of the surface temperature to calculate the snow temperature profile. In the model, the five snow layers are centered at depths of 3.3 cm, 19 cm, 78 cm, 2.7 m, and 7.0 m below the surface. The forcing signal and the corresponding temperature profiles on 6 January for a grid point corresponding closely to the geographical South Pole are given in Fig. 5. In the original ECHAM code, the annual cycle of the surface temperature is prescribed by a cosine function with the same annual mean and range as the climatological annual cycle. Because at high latitudes the annual cycle of the surface temperature is not cosine shaped (long ''coreless'' winter and short ''peaked'' summer), this forcing is a rather poor approximation, as is shown in Fig. 5a. The effect of the different approaches on initialization profiles for 6 January is shown in Fig. 5b. The impact on the initialization profiles is modest in austral summer. Initialization at the end of the long coreless winter results in a much larger difference between the two methods. It

TABLE 1. Short description of the ECHAM4 parameterizations (Roeckner et al. 1996) and the adjustments made before the model was applied to Antarctica.

Parameterization	Description
Surface fluxes and vertical diffusion	Turbulent fluxes at the surface are calculated from Monin–Obukhov similarity theory. Approximate analytical expressions derived by Louis (1979) for the transfer coefficients are used. A higher-order closure is used to compute turbulent transfer within and above the boundary layer. In this formulation eddy diffusivity is expressed in terms of turbulent kinetic energy. The effective roughness length is introduced to account for the effects of subgrid terrain effects and subgrid orography. The effective roughness length is taken from the ECMWF model.
Land surface processes	The heat diffusion equation is solved for five soil layers with zero heat flux at a depth of 10 m. The original ECHAM4 code is adjusted by prescribing heat diffusivity and capacity of snow.
Gravity wave drag	Drag associated with orographic waves is simulated using directionally dependent subgrid-scale orographical variances obtained from the Drewry dataset (Miller et al. 1989).
Cumulus convection	Bulk mass concept for shallow, midlevel, and deep convection (Tiedtke 1989).
Stratiform clouds	Budget equations for water vapor and cloud water (prognostic variable) (Sundqvist 1978).
Radiation	Broadband flux emissivity method with six longwave bands and two-stream formulation with two shortwave intervals (Fouquart and Bonnel 1980; Morcrette et al. 1986). In the ECHAM4 code, the albedo is parameterized as a function of temperature. This however does not agree with albedo measurements. Therefore a constant albedo of 0.8 is prescribed in the adjusted code.

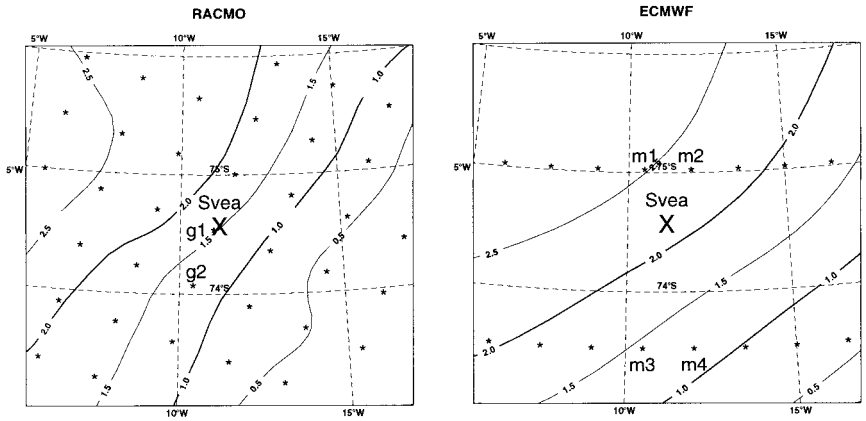

FIG. 4. Location of the two RACMO grid points g_1 and g_2 and the four points m_1–m_4 of the regular latitude–longitude grid on which the ECMWF reanalyses are interpolated. The location of the Swedish research station Svea is indicated by the symbol X. The contour lines represent the surface geopotential height (km) in the two models. RACMO uses the Drewry topography and ECMWF uses the U.S. Navy database. The surface geopotential height at Svea is 1.2 km. The scale of the figure is approximately 350 km × 350 km.

should be noted that even if the Fourier decomposition is used to calculate realistic initialization profiles, these profiles are, most probably, not identical to the real snow temperature profiles in Antarctica at the time of initialization because 1) the initialization of the snow temperature profiles is taken from a climatology of snow surface temperatures, whereas the true snow temperature profiles at a specific moment depend strongly on the meteorological conditions in the preceding weeks, and 2) the accuracy of the database of snow surface temperatures is unknown.

4. Results

In this section, model output and ECMWF reanalyses for the 6-day period 14–19 January 1993 (P1) are evaluated using measurements made at the Swedish research station Svea during the same period. An integration is carried out for the period 6–19 January 1993. The model is initialized with the ECMWF reanalysis of 0000 UTC 6 January 1993. Period P1 is chosen for the evaluation because fair weather conditions allowed for an increase in the frequency of balloon soundings to one sounding per 3 h. From tendencies of the model prognostic variables, it appeared that the atmospheric spinup time is of the order of a few hours.

a. Temperature

1) ATMOSPHERE

The ability of RACMO to simulate the boundary layer temperature profile of a typical Antarctic summer day is studied. In Fig. 6a model output averaged over P1 for the two grid points g_1 and g_2 is plotted together with the observed profiles. Averaged over this period, the

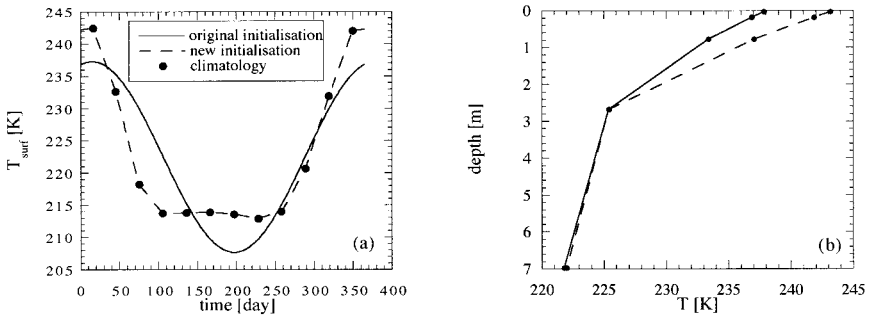

FIG. 5. (a) The large dots represent the climatology of monthly mean surface temperatures for a grid point close to the geographical South Pole. From these climatological values, an annual cycle of the surface temperature is derived with two methods described in the text. These signals are used to calculate the initial snow temperature profiles. The annual mean and the range of both forcings are the same. (b) The initialization temperature of the five snow layers at 6 Jan. The profile derived with the original ECHAM code for snow initialization is indicated with the continuous line and the profile derived with the improved code is indicated with the dashed line.

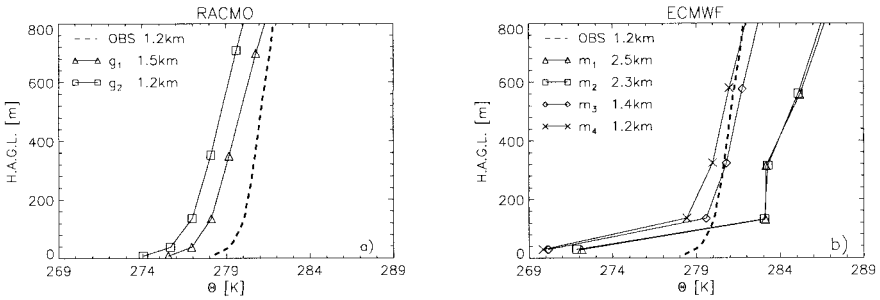

FIG. 6. Mean potential temperature for the period 14–19 Jan 1993 (P1) as a function of height above ground level (H.A.G.L.). The observed profiles are shown together with (a) RACMO output and (b) ECMWF reanalyses. The surface geopotential height of the grid points and the height at Svea are given in the legends.

atmosphere is statically stable at Svea. The vertical temperature gradient is fairly well represented by the model, although the simulated gradient is slightly larger than the observed gradient. It is possible that this difference in temperature gradient is caused by a slight overestimation of the effective albedo for the grid box. The value for snow is employed in the model while some snow-free rock areas are present in the surroundings of Svea.

For an evaluation of the absolute temperatures, the model output of grid point g_2 is analyzed, because the surface geopotential height of this grid point corresponds closely to the surface geopotential height at Svea. Table 2 shows the mean difference (B) and the unbiased root-mean-square (rms) difference (S) in the lowest 800 m of the atmosphere during P1 between the simulated temperature profile at g_2 and the observed profile:

$$B = \overline{\Delta X} = \frac{1}{h}\int_0^h (X_{\text{model}} - X_{\text{obs}})\, dz \quad \text{and} \qquad (4)$$

$$S = [\overline{(\Delta X)^2} - (\overline{\Delta X})^2]^{1/2} = \left[\frac{1}{h}\int_0^h (X_{\text{model}} - X_{\text{obs}} - \overline{\Delta X})^2\, dz\right]^{1/2}, \qquad (5)$$

where $h = 800$ m, X_{model} is the value of variable X simulated by RACMO, and X_{obs} is the observed value. The raw measured data are smoothed and interpolated to equidistant reference heights (van den Broeke and Bintanja 1995). The model output is interpolated linearly to these reference heights and the bias and unbiased rms errors are calculated accordingly, by discretizing Eqs. (4) and (5). Averaged over P1, the temperature observed at Svea is 2.6°C higher than the simulated temperature. In the lowest two atmospheric layers, the modeled temperature is almost 4°C lower than the observed temperature during this period. It has to be noted that the temperature inside the valley, where the cable balloon is launched, is 2°–3°C higher than the temperature on the surrounding plateau (section 2). The model output is representative for the undisturbed regime on the plateau.

In Fig. 6b the ECMWF reanalyzed potential temperatures are plotted together with the measurements. It can be seen that the lowest model layer is decoupled from the remaining atmospheric layers in the reanalyses. Therefore, exchange of heat and moisture between the two lowest model layers is strongly suppressed. During P1, the reanalyzed value for $\partial\Theta/\partial z$ between 30 and 135 m at m_4 is 0.07°C m^{-1}, whereas the measured value is only 0.01°C m^{-1}. Above 200 m the difference between the measurements and the reanalyses is less pronounced. From temperature profiles at two grid points, g_i and g_j, a mean model lapse rate $\overline{\Gamma_{ij}}$ is derived:

$$\overline{\Gamma_{ij}} = \frac{1}{h}\int_0^h -\frac{T_j(z) - T_i(z)}{Z_{\text{srf}j} - Z_{\text{srf}i}}\, dz, \qquad (6)$$

where $h = 800$ m, z is the height above the surface, $T_i(z)$ is the temperature at grid point g_i, and $Z_{\text{srf}i}$ is the surface geopotential height at grid point g_i. The value for $\overline{\Gamma_{12}}$ derived with model output from grid points g_1 and g_2 is 5.6°C km^{-1}. This value is used to calculate a

TABLE 2. First line: The mean difference (B) and the unbiased root-mean-square difference (S) [Eqs. (4) and (5)] between the model output and the observed profiles for potential temperature and specific humidity in the lowest 800 m of the atmosphere during P1. Second, third, and fourth lines: The mean simulated minus the observed or inferred fluxes during P1 (Q_R and F_G, downward = positive; F_{SH} and F_{LA}, upward = positive).

$B(\Theta) = -2.6$°C	$S(\Theta) = 0.5$°C	$B(q) = 0.2$ g kg^{-1}	$S(q) = 0.2$ g kg^{-1}
$Q_R = -1$ W m^{-2}	$F_{\text{SH}} = -1$ W m^{-2}	$F_{\text{LA}} = -3$ W m^{-2}	$F_G = -4$ W m^{-2}
$F_{\text{SW}}\downarrow = -26$ W m^{-2}	$F_{\text{SW}}\uparrow = -20$ W m^{-2}	$F_{\text{SW}} = -5$ W m^{-2}	
$F_{\text{LW}}\downarrow = 6$ W m^{-2}	$F_{\text{LW}}\uparrow = 2$ W m^{-2}	$F_{\text{LW}} = 4$ W m^{-2}	

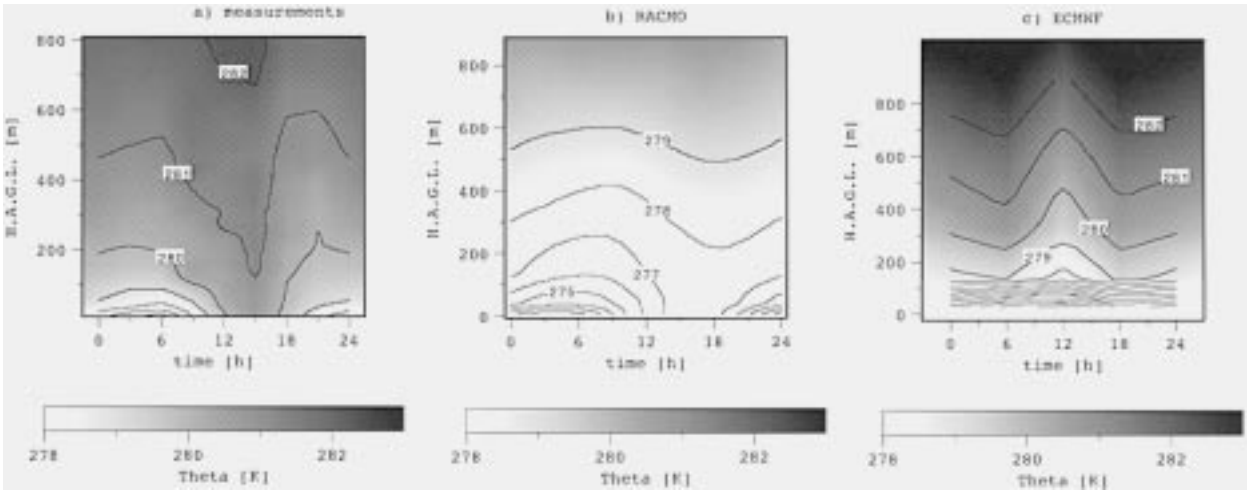

FIG. 7. The mean diurnal cycle of the potential temperature in the boundary layer during P1. The figure shows (a) measurements by pilot balloons at Svea, (b) RACMO output for grid point g_1, and (c) ECMWF reanalyses for grid point m_4. Both RACMO output and ECMWF reanalyses are corrected for the difference in surface geopotential height between the grid point and the measuring site. Note that ECMWF output is only available at 0000, 0600, 1200, and 1800 UTC.

correction for the difference in surface geopotential height between a grid point and the measuring site. Differences between corrected profiles of four grid points surrounding Svea are very small. This makes it plausible that the temperature differences between the grid points are caused mainly by height differences and not by differences in the local circulation. The value for Z_{srf} at g_1 is 269 m larger than Z_{srf} at Svea, so 1.5°C is added to the temperatures at this grid point. The value for $\overline{\Gamma}_{34}$ in the ECMWF reanalyses is 6.4°C km^{-1}. For m_4, 0.4°C is subtracted from the reanalyzed temperatures, because Z_{srf} at this grid point is 63 m lower than Z_{srf} at Svea.

Figure 7 shows the mean measured, simulated, and reanalyzed diurnal cycle of the potential temperature profiles. The ECMWF reanalyses are only available every 6 h. The period of negative net radiation is referred to as nighttime, but it should be borne in mind that the sun is above the horizon 24 h per day. RACMO simulates the daily cycle of the temperature fairly well. The simulated amplitude of the temperature signal is smaller than the observed amplitude above 200 m. This indicates that the model underestimates the energy transport in the boundary layer. As for the case of the averaged profiles, it is found that the simulated lapse rate is slightly too large. The moment when the simulated temperature reaches its maximum value is simulated somewhat too late, especially in the upper parts of the boundary layer.

Figure 7c shows that the ECMWF model fails to reproduce the daily cycle of the boundary layer temperature profiles. Above 100 m, the daily cycle is out of phase with the incoming solar radiation and the minimum temperature is found at roughly 1200 UTC. The exchange coefficient between the two lowest model layers is very small due to decoupling of the lowest model layer from the remaining atmospheric layers.

Differences between RACMO output and ECMWF reanalyses are caused by 1) the assimilation of data in the reanalyses or 2) differences between RACMO and the ECMWF model. Data assimilation plays a minor role at the grid points corresponding most closely to Svea. After all, this site is located at a considerable distance from any station from which observations are assimilated in the reanalysis. Therefore, the differences between RACMO and the ECMWF model physics are likely to be responsible for the differences found in the model output, in particular the differences in the vertical diffusion schemes used. In ECMWF the vertical diffusion is based on the eddy diffusivity concept (K theory). The eddy diffusivity is parameterized as a function of shear, mixing length, and stability functions of the Richardson number. The parameterizations used in RACMO are taken from the global ECHAM4 model. In the ECHAM4 scheme a 1.5-order closure is used. The eddy diffusivity is expressed in terms of turbulent kinetic energy, mixing length, and stability functions. The stability functions differ from the ones used in the ECMWF scheme. In stable situations occurring in this period at Svea, the shear is typically 0.05 s^{-1} and the turbulent kinetic energy is typically 0.5 m^2 s^{-2}. With a value of 2 for the bulk Richardson number, the eddy diffusivity coefficient in the RACMO scheme appears to be roughly three times as large as the coefficient in the ECMWF scheme. The enhancement of heat exchange in stable conditions in RACMO results in a better agreement between simulation and measurements. Nevertheless, the profiles suggest that the heat exchange generated with the ECHAM4 scheme is still insufficient. Another difference between the ECMWF model and RACMO is the value of the absorption coefficients for the water vapor continuum in the radiation code. However, the results of a simulation with RACMO employ-

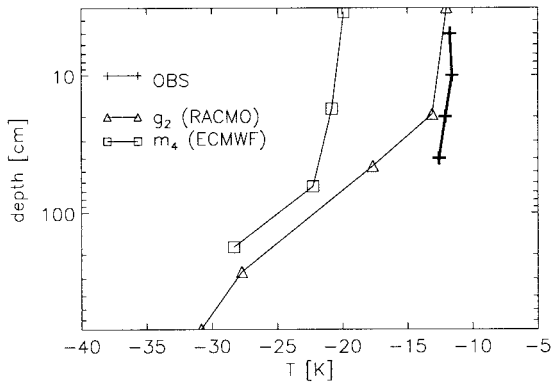

FIG. 8. Measured and simulated temperature as a function of depth in the snow averaged over P1 for RACMO grid point g_2 and ECMWF grid point m_4, corrected for the difference in surface geopotential height between the grid point and the measuring site.

ing the absorption coefficients of the ECMWF model indicated that the difference in the radiation code cannot be the sole explanation for the differences found between the two models in the simulated temperature profiles.

2) SNOW

Figure 8 shows the mean measured and simulated snow temperatures. Above a depth of 20 cm the difference between simulated and measured snow temperatures is small. Evaluation of the atmospheric profiles already showed that RACMO slightly underestimates the temperature near the surface, so the temperature difference between the snow and the lowest model layer is slightly too small in the model. The model clearly underestimates the temperatures in the snow below 20 cm. This is caused by the snow temperature initialization. From a sensitivity study it appears that a difference of 10°C in snow temperature initialization has only an effect of the order of 2°C on the absolute temperature in the boundary layer. The ECMWF reanalyses are roughly 10°C too cold.

In Fig. 9 the measured and simulated daily cycle of the snow temperatures is shown. The observed amplitude of the daily cycle at 5-cm depth is 6.1°C and the simulated amplitude at this depth is 7.5°C. The overestimation of the amplitude can have two causes, namely, 1) the daily variation of the downward flux from the top snow layer to deeper layers is too small due to an underestimation of the diffusivity in the snow or 2) the daily variation of the fluxes at the interface between atmosphere and snow is too large. After all, the temperature tendency in the top snow layer is determined by the flux divergence over that layer. The results of a run performed with the diffusivity introduced in section 3b ($\kappa = 6.06 \times 10^{-7}$ m^2 s^{-1}) being replaced by the observed diffusivity at Svea ($\kappa = 3.11 \times 10^{-7}$ m^2 s^{-1}) overestimate the amplitude of the daily cycle even more. In section 4c we discuss the simulated amplitude of the daily cycle at the interface between the atmosphere and snow. The amplitude of the surface temperature signal in the ECMWF reanalyses is in good agreement with the amplitude of the measured daily cycle but far too cold (Fig. 9c).

b. Humidity

The exchange coefficient for moisture is a function of the temperature gradient in the atmosphere. Therefore, to obtain the correct humidity profile it is essential that at least the temperature profile is simulated properly. The average simulated specific humidity in the lowest 800 m of the atmosphere is 0.2 g kg^{-1} larger than the observed specific humidity (Table 2). Near the surface, the difference is largest (0.3 g kg^{-1}). Although the difference between the simulated and the observed vertical temperature gradients is not large, a consider-

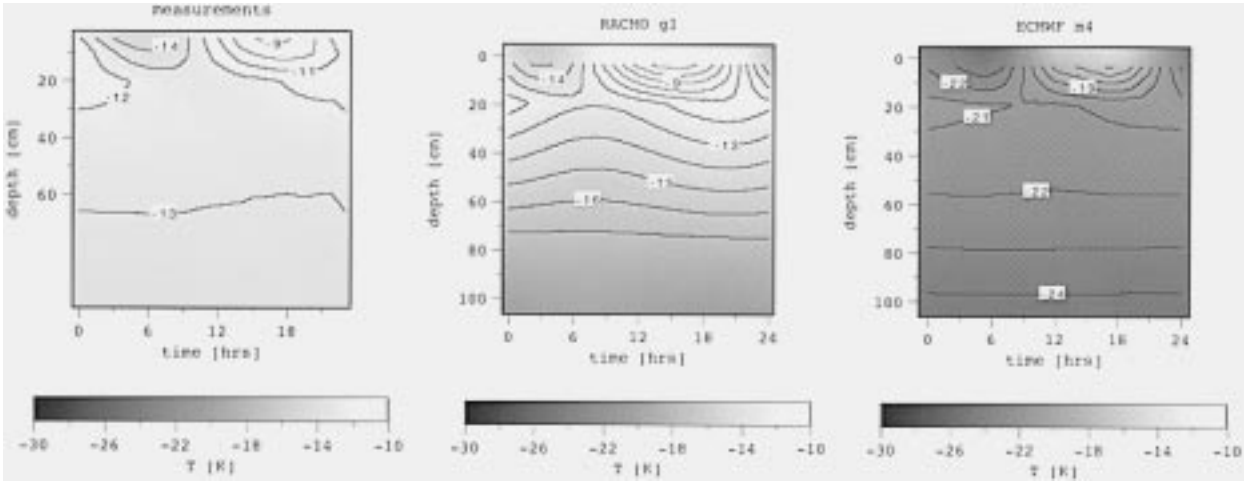

FIG. 9. Similar to Fig. 7 but for temperature in the snow.

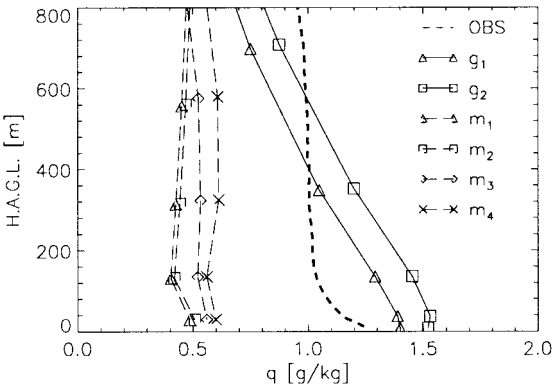

FIG. 10. Mean specific humidity during P1. The observed profiles are shown together with RACMO output for the grid points g_1 and g_2 and ECMWF reanalyses for the grid points m_1–m_4.

able difference in vertical humidity gradient is present (Fig. 10). The observations show that the specific humidity at Svea decreases with height in the lowest 100 m of the atmosphere but remains constant from 100 to 800 m. However, this is not reproduced by the model. The simulated specific humidity decreases with height in the lowest 800 m. The absolute amount of water vapor is too small in the ECMWF reanalyses, but the vertical humidity gradient corresponds surprisingly well to the observations. However, the upward moisture flux at 100 m is probably largely underestimated due to the decoupling of the lowest model layer from the remaining layers. The underestimation of this flux is a possible explanation for the small gradient in the specific humidity.

Figure 11 shows the observed, simulated, and reanalyzed mean daily cycle in the specific humidity. The simulated amplitude of the humidity signal below 200 m is far too large. During the night, the simulated specific humidity even increases with height below 136 m and reaches a maximum value at this level, because the latent heat flux is directed downward. This is not observed at Svea. The simulated latent heat flux is directed downward because the simulated specific humidity in the atmosphere exceeds the saturation specific humidity corresponding to the surface temperature [$q_{\text{sat}}(T_s)$]. This happens because the amplitude of the surface temperature signal is overestimated by the model. Figure 11c shows that in the ECMWF reanalyses the variation of specific humidity is much smaller than in the result obtained with RACMO, but it should be borne in mind that the reanalyses are only available every 6 h. As in Fig. 10, the decrease in specific humidity with height during the night is also much smaller than in the RACMO simulation.

c. Surface fluxes

The flux divergence in the boundary layer is one of the terms in the temperature and humidity tendency equation. Therefore, a comparison between simulated and observed surface fluxes gives us a better understanding of the difference between simulated and observed temperature and humidity profiles. At the interface between the snow and the atmosphere the net radiative flux (Q_R; downward = positive) is balanced by the soil heat flux (F_G; downward = positive) and the turbulent fluxes (latent heat flux F_{LA} and sensible heat flux F_{SH}; upward = positive), so the energy balance at the surface is given by

$$Q_R = F_G + F_{\text{LA}} + F_{\text{SH}}. \tag{7}$$

The net radiative flux (Q_R) is the sum of the individual components, namely downward and upward shortwave radiation ($F_{\text{SW}}\downarrow$ and $F_{\text{SW}}\uparrow$) and downward and upward longwave radiation ($F_{\text{LW}}\downarrow$ and $F_{\text{LW}}\uparrow$). The soil heat flux

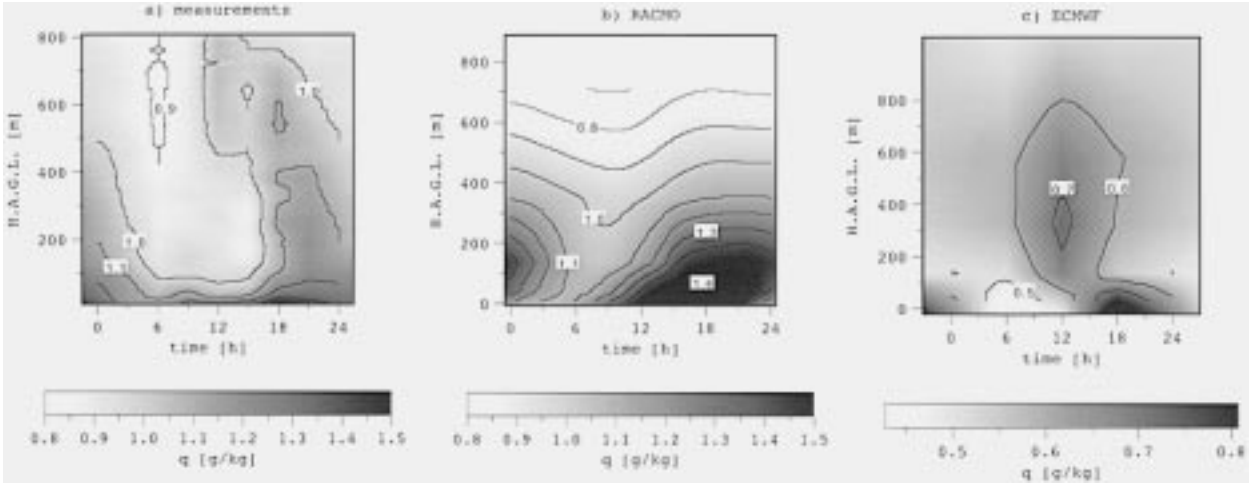

FIG. 11. The mean diurnal cycle of the specific humidity in the boundary layer during P1. The figure shows (a) measurements by cable balloons at Svea, (b) RACMO output for grid point g_1, and (c) ECMWF reanalyses for grid point m_4. Note that ECMWF output is only available at 0000, 0600, 1200, and 1800 UTC.

(F_G) is available for temperature changes in the five snow layers.

Figure 12 depicts the measured/inferred and modeled mean daily cycle of the surface fluxes during P1. In general, the model is able to simulate the daily cycle of the surface fluxes properly. However, if one looks in more detail, differences between modeled and measured/inferred fluxes can be identified. In Table 2 the mean differences during P1 between simulated and measured/inferred fluxes are given. We now discuss these differences.

1) SHORTWAVE RADIATION

The simulated incoming and outgoing shortwave fluxes are underestimated by 26 W m^{-2} and 20 W m^{-2}, respectively, due to an overestimation of the cloud cover in the model. Clouds were generated by the model between 0.4 and 7.4 km with a maximum mean cloud cover of 1.2 octas at a height of 2.7 km, whereas during P1 a mean cloud cover of less than 0.5 octas was observed at Svea. Due to the high albedo, the difference between simulated and observed net shortwave radiation is only 5 W m^{-2}. In the next section the results of a sensitivity run are discussed with the cloud feedback to the radiation switched off.

2) LONGWAVE RADIATION

The mean simulated incoming longwave radiation at the surface is 6 W m^{-2} larger than the inferred flux. This difference is on the order of the uncertainty in the inferred fluxes, so hardly significant. Probably, the effects on $F_{LW}\downarrow$ of 1) an overestimation of the cloud cover and 2) an overestimation of the specific humidity near the surface are partly compensated for by the effect of 3) an underestimation of the temperature near the surface. Larger differences can be identified for the separate time intervals. Averaged over the period from 1800 to 2400 UTC, a significant overestimation of $F_{LW}\downarrow$ by 25 W m^{-2} is present. The third model feature, namely the underestimation of the temperature near the surface is smaller during this time interval so that the two other points dominate, resulting in an overestimation of the flux.

3) OTHER FLUXES

The mean simulated net radiative flux corresponds closely to the inferred flux. Substantial differences between modeled and inferred fluxes are, however, present within certain time intervals. During the time interval from 0000 to 0600 UTC, Q_R is underestimated by 15 W m^{-2}, which is entirely compensated for by an overestimation of the downward turbulent heat flux by 14 W m^{-2} during this interval. The mean heat flux into the snow is simulated within the bounds of uncertainty in the inferred fluxes. However, the simulated amplitude of the daily cycle of F_G is larger than the inferred amplitude. As a consequence, the amplitude of the surface temperature signal is overestimated.

5. Sensitivity experiments

Sensitivity runs have been performed to study the impact of the modifications to the original code as described in section 3. Table 3 summarizes the sensitivity experiments. In all sensitivity runs, the cloud feedback in the radiation is ignored at all grid points and for the entire period of the simulation. The reason is twofold: 1) the cloud cover in a sensitivity run can differ largely from the cloud cover in the reference run, which makes it very difficult to interpret the results, and 2) in the reference run described in section 4, a mean cloud cover of 1.2 octas at a height of 2.7 km was simulated, whereas during P1, a mean cloud cover of less than 0.5 octas was observed at Svea. But even when the cloud feedback in the radiation calculations is ignored, it remains quite difficult to interpret differences between the various sensitivity runs, because a large number of complex feedback mechanisms are present in the model. For example, a model parameter can have an impact on the wind speed, which is important for the surface fluxes and the turbulent heat exchange in the atmosphere. This again has an impact on other meteorological variables like temperature and humidity.

The reference run, described in section 4, will be referred to as REF. A control run (CTL) is carried out, in which radiation calculations are performed for cloud-free conditions. In this section, the sensitivity runs are compared with the CTL run. Table 4 shows the mean difference and the unbiased root-mean-square difference [Eqs. (4) and (5)] in the lowest 800 m of the atmosphere during P1 between the simulated temperature and humidity profiles at g_2 and the observed profiles. In Table 5 the mean difference during P1 between the simulated and the measured surface fluxes is given. Table 6 shows the mean difference and the unbiased rms difference between the sensitivity runs and the CTL run for temperature and specific humidity. The variables are calculated as in Eqs. (4) and (5) but with $h = 1200$ m. Table 7 shows the mean difference between the surface fluxes in the sensitivity runs and the surface fluxes in the CTL run.

a. Clouds

By comparing REF with CTL, we can study whether the differences between REF output and the observations can be explained by the effect of overestimating the cloud amount. It is also possible that a model deficiency is compensated for by the effect of overestimating the cloud amount. Clouds have a large impact on the distinct components of the net radiative flux (Table 7). Shortwave radiation is reflected by clouds. Therefore, the shortwave fluxes at the surface are much small-

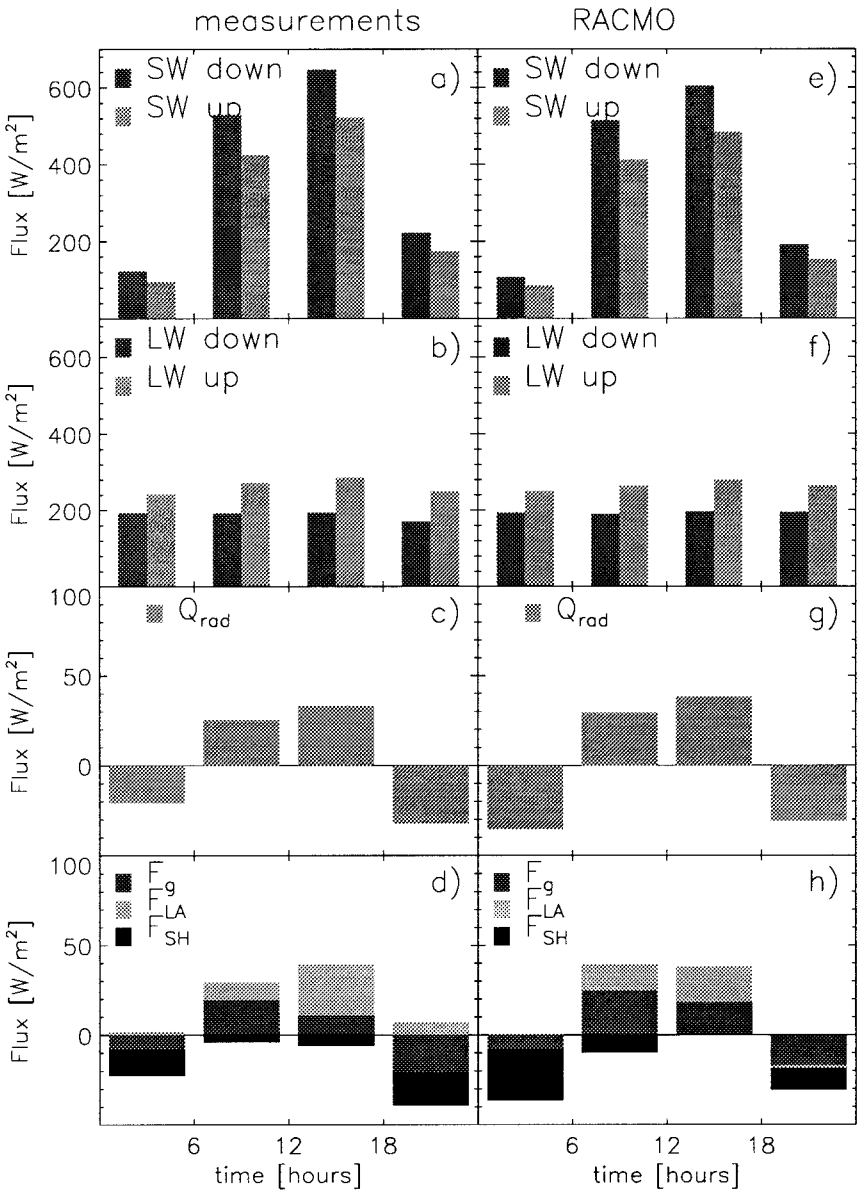

FIG. 12. Diurnal cycle of the surface fluxes during P1 inferred from measurements at Svea site 4 (a)–(d) and simulated at grid point g_2 (e)–(h) (Q_R and F_G, downward is positive; F_{SH} and F_{LA}, upward is positive).

TABLE 3. Overview of the sensitivity runs. The run described in section 4 is referred to as the REF run. In this run the impact of clouds on the radiative fluxes is taken into account. In the other runs the radiation calculations are performed for cloud-free conditions.

REF	Reference run. This is the only run in which the impact of clouds on the radiative fluxes is taken into account.
ALB	Albedo is parameterized as a function of temperature as in the ECHAM4 code [Eq. (1)].
ICE	Values of ice for κ and ρC_g are used as in the ECHAM4 code.
LEVM	Nineteen layers in the vertical.

TABLE 4. The mean difference (B) and the unbiased rms difference (S) [Eqs. (4) and (5)] between the sensitivity runs and the observed profiles for potential temperature (°C) and specific humidity (g kg^{-1}) in the lowest 800 m of the atmosphere during P1. The run described in section 4 is referred to as the REF run.

	REF	CTL	ALB	ICE	LEVM
$B(\Theta)$	−2.6	−4.3	−3.6	−4.9	−2.7
$S(\Theta)$	0.5	1.0	0.6	1.4	0.5
$B(q)$	0.2	−0.2	0.0	−0.4	0.1
$S(q)$	0.2	0.2	0.2	0.1	0.2

TABLE 5. The mean simulated fluxes minus observed or inferred fluxes (W m^{-2}) during P1 (Q_R and F_G, downward = positive; F_{SH} and F_{LA}, upward = positive).

	REF	CTL	ALB	ICE	LEVM
$F_{SW}\downarrow$	−26	15	13	13	10
$F_{SW}\uparrow$	−20	12	7	11	8
F_{SW}	−5	3	6	2	2
$F_{LW}\downarrow$	6	−20	−15	−21	−9
$F_{LW}\uparrow$	2	−10	−6	−13	−6
F_{LW}	4	−10	−9	−8	−3
Q_R	−1	−7	−3	−5	−2
F_{SH}	−1	−6	−2	−12	2
F_{LA}	−3	−3	−4	−4	−6
F_G	4	3	3	11	3

er in the REF run. In REF, $F_{SW}\downarrow$ and $F_{SW}\uparrow$ are underestimated by 26 W m^{-2} and 20 W m^{-2}, respectively, whereas these fluxes are overestimated in CTL by 15 W m^{-2} and 12 W m^{-2}, respectively (Table 6). Obviously, a cloud cover that lies in between the REF cloud cover and zero gives shortwave fluxes at the surface that are in good agreement with the observations. The inclusion of the radiative effect of clouds yields a 26 W m^{-2} larger value for $F_{LW}\downarrow$. Not only is the optical depth of a cloudy sky larger than that of a clear sky, but in addition, when the radiative effect of clouds is included, the boundary layer temperatures are higher, and the specific humidity in the boundary layer is larger. It appears that an underestimation of the downward longwave clear-sky radiation at the surface is compensated for by an overestimation of the cloud cover. Other models have also problems with underestimated downward longwave radiation over Antarctica. King and Connolley (1997) found an underestimation of the longwave radiation of about 20 W m^{-2} in the U. K. Meteorological Office unified climate model. In REF, $F_{LW}\uparrow$ is larger because the surface temperature is higher. Altogether, the impact of clouds on F_{LW} at the surface is compensated partly by the impact of clouds on F_{SW}. Therefore, Q_R is only 6 W m^{-2} larger when the radiative effect of clouds is included. The difference is balanced mainly by the difference in F_{SH}. In the presence of clouds there is less sensible heat exchange between the snow and the atmosphere.

In REF, the mean potential temperature below 1200 m is 1.5°C higher (Table 6), implying that simulated clouds have a warming effect on the boundary layer, which is consistent with a smaller turbulent heat exchange between the surface and the boundary layer in the presence of clouds. The difference in boundary layer temperature between REF and the observations would have been larger if the cloud cover had not been overestimated in this run. Figure 13a shows the REF, CTL, and measured mean potential temperature profiles. The simulated cloud cover hardly affects the vertical temperature gradient. From Fig. 13b, it can be seen that the impact of clouds on the vertical humidity gradient is small, so the bias in this gradient cannot be explained by spurious clouds. In REF, the humidity below 1200 m is 0.3 g kg^{-1} larger than in CTL, whereas the difference in surface latent heat flux is negligible.

TABLE 6. The mean difference (B) and the unbiased rms difference (S) [Eqs. (4) and (5)] during P1 between the sensitivity runs and the control run for potential temperature (°C) and specific humidity (g kg^{-1}) in the lowest 1200 m of the atmosphere.

	REF	ALB	ICE	LEVM
$B(\Theta)$	1.5	0.3	−0.5	1.2
$S(\Theta)$	0.6	0.7	0.5	0.7
$B(q)$	0.3	0.2	−0.1	0.4
$S(q)$	0.0	0.0	0.2	0.1

b. The albedo parameterization

In CTL, a constant albedo of 0.8 is prescribed for all land points. In the sensitivity run ALB, the albedo is parameterized as in the ECHAM4 code according to Eq. (1). Differences can only be expected for snow-covered land points when the surface temperature exceeds −10°C.

In Fig. 14, the ALB fluxes minus the CTL fluxes are shown. The largest differences occur during the time interval I3 from 1200 to 1800 UTC. During I3, the simulated surface temperature exceeds −10°C at Svea and the parameterized albedo in the ALB run decreases. Therefore, more net shortwave radiation is available at the interface between the snow and the atmosphere. This surplus is divided mainly over F_{SH} and F_G. During I3, there is a large difference between the inferred fluxes and the ALB fluxes. In ALB, the surface temperature becomes higher than the atmospheric temperature of the lowest model layer during I3; hence, the sensible heat flux (F_{SH}) is directed upward, which is opposite to the inferred F_{SH}. In addition, the simulated heat flux into the snow is 15 W m^{-2} larger during I3 than the inferred flux. The daily variation of F_G, which was already overestimated in CTL, is even larger in ALB. Averaged over the entire period, the ALB turbulent heat fluxes are smaller, which is consistent with a lower wind speed in the lowest model layer. The mean potential temperature

TABLE 7. The mean fluxes simulated with the parameters used in the sensitivity runs minus the fluxes simulated with the control parameters (W m^{-2}) during P1 (Q_R and F_G, downward = positive; F_{SH} and F_{LA}, upward = positive).

	REF	ALB	ICE	LEVM
$F_{SW}\downarrow$	−40.4	−1.6	−1.3	−5.0
$F_{SW}\uparrow$	−32.3	−5.0	−1.1	−4.0
F_{SW}	−8.1	3.4	−0.2	−1.0
$F_{LW}\downarrow$	26.0	4.2	−1.3	10.6
$F_{LW}\uparrow$	11.8	3.8	−3.4	4.1
F_{LW}	14.2	0.4	2.1	6.6
Q_R	6.1	3.8	1.9	5.6
F_{SH}	4.6	4.1	−5.8	7.9
F_{LA}	0.3	−0.9	−0.4	−2.9
F_G	1.2	0.6	8.1	0.6

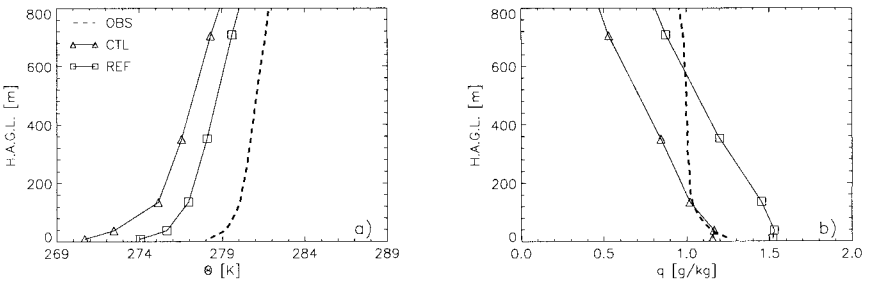

FIG. 13. Average values during P1 of (a) potential temperature and (b) specific humidity. The measured profiles are shown together with the profiles simulated with the CTL and with the REF parameters at grid point g_2.

in the lowest 1200 m of the atmosphere is 0.3°C higher in the ALB run than in the CTL run (Table 6), which is consistent with the smaller absolute value for F_{SH} in the ALB run. The vertical gradient in specific humidity is roughly the same in the two runs, but the absolute value for the specific humidity is 0.2 g kg^{-1} larger in the ALB run (Table 6).

c. The heat capacity and diffusivity of snow

In the CTL run, a heat capacity (ρC_g) of 0.804×10^6 J m^{-3} K^{-1} and a diffusivity (κ) of 6.06×10^{-7} m^2 s^{-1} are prescribed to calculate the heat exchange between the five soil layers (section 3b). In the ECHAM4 code, the values for ice ($\rho C_g = 2.09 \times 10^6$ J m^{-3} K^{-1}, $\kappa = 12 \times 10^{-7}$ m^2 s^{-1}) are used. In the sensitivity run ICE, the original ECHAM4 values are reimplemented to study the impact of variations in these parameters on the simulated boundary layer profiles and on the surface fluxes.

In Fig. 15, the simulated and inferred surface fluxes F_{SH}, F_{LA}, and F_G are shown. Clearly, the CTL fluxes compare much better with the inferred fluxes than the ICE fluxes. In ICE, the daily variation of F_G is much larger than the variation measured at Svea. The overestimation of this variation is a result of the overestimation of the diffusivity in the snow. In ICE, the mean downward sensible heat flux is 6 W m^{-2} larger than in CTL, resulting in a 0.5°C lower boundary layer temperature (Fig. 16). In addition, a larger temperature gradient between the layers at 37 and 134 m is present in ICE. Therefore, the exchange coefficients between these layers are small, giving rise to a large humidity gradient. Moisture that has evaporated from the surface remains in the lowest two layers of the atmosphere, restricting evaporation during the day. Contrary to CTL, the latent heat flux in ICE is directed upward during the night, due to a smaller amplitude of the daily cycle of the surface temperature and of the temperature of the lowest atmospheric layers.

We conclude that replacing the ice-type values for κ and ρC_g as being used in the ECHAM model by snow-type values as introduced in section 3b yields a large improvement in simulating the surface fluxes and boundary layer profiles.

d. The height of the lowest model layer

Originally, the lowest model layer was centered around 30 m, which is a typical value being used in

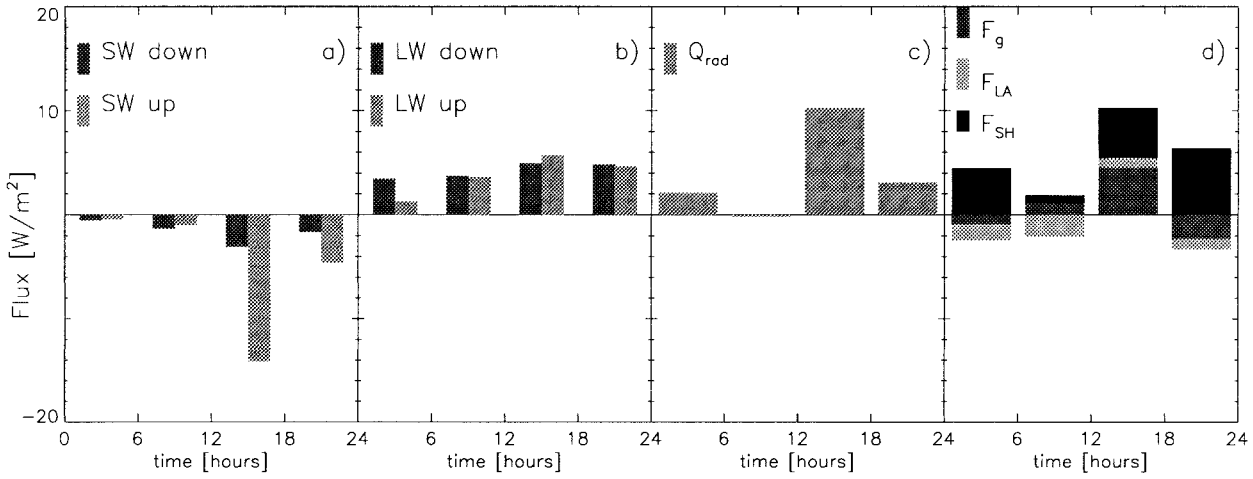

FIG. 14. Difference between the mean CTL fluxes and the mean ALB fluxes at grid point g_2 during P1.

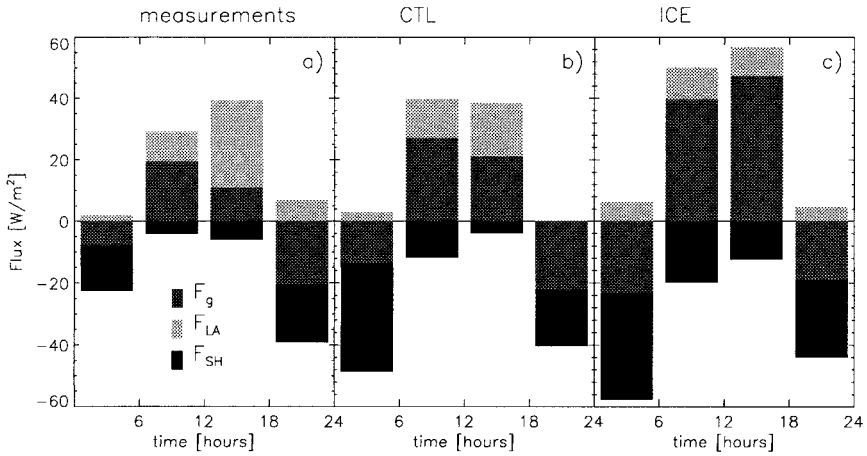

FIG. 15. Mean diurnal cycle of turbulent heat fluxes at the surface and heat flux into the snow during P1 (a) inferred from measurements at Svea, (b) simulated at grid point g_2 with the CTL, and (c) with the ICE parameters.

present-day large-scale atmospheric models. In all the simulations discussed up to here, an additional layer, centered at a height of roughly 8 m, was inserted in order to resolve the shallow boundary layer in more detail. The effect of leaving out this very shallow layer and thus returning to a more standard vertical resolution was studied with the sensitivity run LEVM.

In Fig. 17 the mean potential temperature profiles are shown. In LEVM, the vertical gradient in the temperature profile is smaller than in CTL. The stable layer near the surface is resolved in less detail. The turbulent heat fluxes at the surface are smaller, because of the weaker coupling between the lowest atmospheric layer and the surface. The downward sensible heat flux is 8 W m^{-2} smaller, leading to a 1.2°C warmer boundary layer. Radiation loss during the night is balanced mainly by F_{SH} and F_G. Because F_{SH} is smaller in LEVM, the upward directed F_G has to be larger during the night. During the day, less evaporation takes place in LEVM, so the incoming radiation is available for the downward directed F_G. Altogether, the amplitude of the daily cycle of F_G is larger in LEVM, resulting in a larger amplitude of T_s. The specific humidity in the boundary layer is larger in the LEVM run, but the vertical gradient in specific humidity is similar in the two runs.

The insertion of an extra shallow model layer near the surface does not result in a better or poorer correspondence between simulation and observation. However, the results show that the stable boundary layer is better resolved with an additional shallow layer near the surface.

6. Summary

In this paper, we have studied the correspondence between boundary layer profiles, surface fluxes, and snow temperatures obtained from in situ measurements made at Svea (Antarctica) and the output of a regional atmospheric model (RACMO). The model is driven from the lateral boundaries by ECMWF reanalyses. The reference version of the model carries the parameterization package for the physical processes from the ECHAM4 GCM, with a few adjustments being made for the purpose of simulating typical Antarctic conditions.

The simulated temperatures are in good agreement with the temperatures measured at Svea. The simulated temperature in the boundary layer is 2°–3°C lower than the measured temperature. Negative biases as well as positive biases are found in studies with GCMs. For

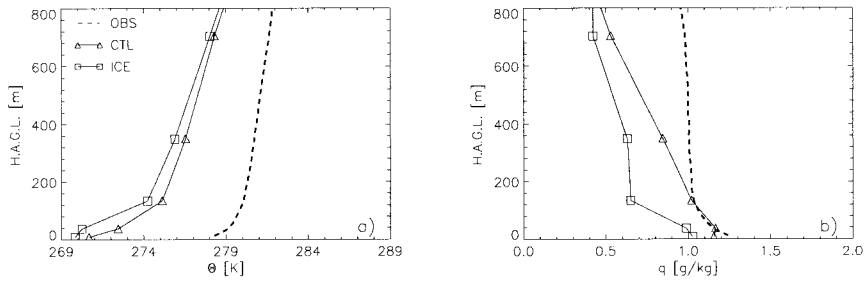

FIG. 16. Similar to Fig. 13 but the CTL run is replaced by the ICE run.

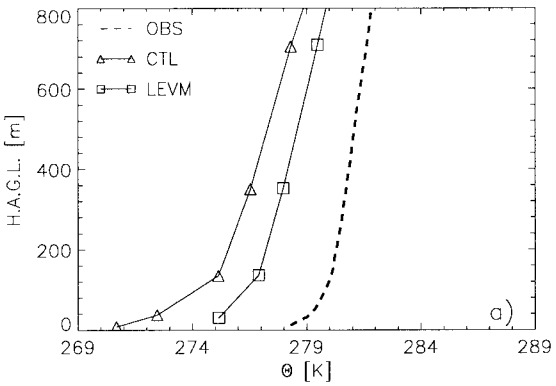

FIG. 17. Similar to Fig. 13a but the CTL run is replaced by the LEVM run.

example, van den Broeke (1997) found that the differences in surface temperature between automated weather station measurements and model output of the global ECHAM model are within a range of −3° to 3°C. RACMO overestimates the daily variation of temperature below 200-m height and underestimates this variation above 200-m height, indicating that the simulated turbulent heat exchange in the atmosphere is too small. The cloud cover at Svea is overpredicted. Results from a sensitivity study show that the simulated boundary layer temperature is reduced by 1.5°C when the feedback of clouds to the radiative fluxes is not taken into account. Thus, the underestimation of the boundary layer temperature is partly canceled by the warming effect of an overpredicted cloud amount. Enhancement of the surface temperature due to spurious clouds is also found in other atmospheric models. Hines et al. (1997) showed that in DARLAM excessive moisture leads to excessive atmospheric back radiation resulting in a large overestimation of the surface temperature. The simulated amount of water vapor in the boundary layer depends largely on the different parameters in RACMO. After all, the difference in specific humidity between the sensitivity runs is large. However, in any of these simulations, the decrease in specific humidity with height is too large. This indicates that the simulated turbulent transport of moisture to higher atmospheric layers is too small. On the other hand, the turbulent heat fluxes at the surface are simulated quite well as they fall within the bounds of uncertainty of the measurements. This applies also to the radiative fluxes at the surface, except for the separate components of the shortwave radiative flux. The latter is due to an overprediction of cloud amount. The daily variation of the heat flux into the snow is too large. This in turn generates a too large daily variation of the temperature in the top snow layer.

The temperature gradient in the boundary layer at Svea is largely overestimated by the ECMWF reanalyses. The lowest atmospheric layer is decoupled from the remaining atmospheric layers. Due to this decoupling, turbulent transport of heat and moisture to higher atmospheric layers is very small. As a consequence, the daily cycle of the temperature in the atmospheric layers above the lowest model layer is not simulated properly by the ECMWF model. Despite the decoupling, the specific humidity gradient in the boundary layer corresponds surprisingly well to the observed gradient. Fortunately, the usefulness of the ECMWF reanalyses in our study is not jeopardized by these findings. Apart from the initialization the reanalyses are only used to relax the atmospheric prognostic variables of RACMO in the boundary zone of the model domain. This boundary is located entirely over the ocean, where the temperature profiles in the ECMWF reanalyses appear to be quite realistic.

Addition of a shallow model layer near the surface at a height of approximately 8 m neither improves nor degrades the overall correspondence between model output and the observations. On the other hand, temperature profiles near the surface are clearly better resolved when the additional shallow layer is present. The adjustments in albedo parameterization and the characteristics of the snow contribute to a better correspondence between the model output and the observations. In the run using the original ECHAM albedo parameterization, the net radiation at the surface is too large during the time interval from 1200 to 1800 UTC. This is related to a reduction of the albedo during this time interval. In a run with the original ECHAM coefficients for the diffusivity and heat capacity in the soil, the daily variation of the net radiative surface fluxes and the heat flux into the snow are largely overestimated.

We showed that the simulated fluxes are consistent with the simulated boundary layer profiles. Turbulent transport is probably somewhat underestimated by the model, but the difference between the model output and measurements is small. The boundary layer is 2.6°C colder and 0.2 g kg^{-1} wetter than the measurements indicate and the net surface heat fluxes are simulated within the bounds of the uncertainty in the measurements. An earlier study performed by van Lipzig et al. (1998) showed that the temperature and humidity profiles at the South Polar station and the Georg-von-Neumayer station are simulated within 5°C and 0.5 g kg^{-1}, respectively, in the entire atmospheric column. From these results, we conclude that RACMO can be used in longer integrations.

Acknowledgments. Members of the ice and climate group of IMAU and of the atmospheric research group of KNMI are thanked for useful comments. The authors thank the ECMWF staff for their help in obtaining and interpreting the ECMWF reanalyses. Sheila McNab corrected the English of this paper. This work was sponsored by the National Computing Facilities Foundation for the use of supercomputer facilities and with financial support from the Netherlands Antarctic Research Programme.

REFERENCES

Beljaars, A. C. M., 1995: The impact of some aspects of the boundary layer scheme in the ECMWF model. *Proc. Parametrization of Sub-Grid Scale Physical Processes*, Reading, United Kingdom, ECMWF, 125–161.

Bintanja, R., and M. R. van den Broeke, 1995: The surface energy balance of Antarctic snow and blue ice. *J. Appl. Meteor.*, **34,** 902–926.

——, ——, and M. J. Portanger, 1993: A meteorological and glaciological experiment on a blue ice area in the Heimefront Range, Queen Maud Land, Antarctica. Svea Field Report, Institute for Marine and Atmospheric Research Utrecht, Utrecht University, 29 pp. [Available from IMAU, P. O. Box 80005, 3508 TA Utrecht, Netherlands.]

Bromwich, D. H., F. M. Robasky, R. I. Cullather, and M. L. Woert, 1995: The atmospheric hydrological cycle over the Southern Ocean and Antarctica from operational numerical analyses. *Mon. Wea. Rev.*, **123,** 3518–3538.

Budd, W. F., P. A. Reid, and L. J. Minty, 1995: Antarctic moisture flux and net accumulation from global atmospheric analyses. *Ann. Glaciol.*, **21,** 149–156.

Christensen, J. H., O. B. Christensen, P. Lopez, E. van Meijgaard, and M. Botzet, 1996: The HIRHAM4 regional atmospheric climate model. DMI Scientific Rep. 96-4, Copenhagen, Denmark, 51 pp. [Available from DMI, Lyngbyvej 100, DK-2100 Copenhagen, Denmark.]

——, B. Machenhauer, R. G. Jones, C. Schär, P. M. Ruti, M. Castro, and G. Visconti, 1997: Validation of present-day regional climate simulations over Europe: LAM simulations with observed boundary conditions. *Climate Dyn.*, **31,** 489–506.

Connolley, W. M., and H. Cattle, 1994: The Antarctic climate of the UKMO unified model. *Antarct. Sci.*, **6,** 115–122.

Cullather, R. I., D. H. Bromwich, and R. W. Grumbine, 1997: Validation of operational numerical analyses in Antarctic latitudes. *J. Geophys. Res.*, **102** (D12), 13 761–13 784.

Dethloff, K., A. Rinke, R. Lehmann, J. H. Christensen, M. Botzet, and B. Machenhauer, 1996: Regional climate model of the Arctic atmosphere. *J. Geophys. Res.*, **101,** 23 401–23 422.

Dickinson, R. E., R. M. Errico, F. Giorgi, and G. T. Bates, 1989: A regional climate model for the western United States. *Climate Change*, **15,** 383–422.

Drewry, D. J., 1983: *Antarctica: Glaciological and Geophysical Folio.* Scott Polar Research Institute, 9 maps.

Engels, R., and G. Heinemann, 1996: Three-dimensional structures of summertime Antarctic mesoscale cyclones: Part II: Numerical simulations with a limited area model. *Global Atmos. Ocean Syst.*, **4,** 181–208.

Fouquart, Y., and B. Bonnel, 1980: Computation of solar heating of the earth's atmosphere: A new parameterization. *Beitr. Phys. Atmos.*, **53,** 35–62.

Genthon, C., 1994: Antarctic climate modeling with general circulation models of the atmosphere. *J. Geophys. Res.*, **99** (D6), 12 953–12 961.

——, and A. Braun, 1995: ECMWF analyses and predictions of the surface climate of Greenland and Antarctica. *J. Climate*, **8,** 2324–2332.

Gibson, R., P. Kållberg, S. Uppala, A. Hernandez, A. Nomura, and E. Serrano, 1997: ERA description. ECMWF Re-Analysis Project Rep. Series 1, Reading, United Kingdom, 72 pp.

Gustafsson, N., 1993: HIRLAM 2 final report. HIRLAM Tech. Rep. 9, SMHI, Norrköping, Sweden, 126 pp. [Available from SMHI, S-60176 Norrköping, Sweden.]

Heinemann, G., 1997: Idealized simulations of the Antarctic katabatic wind system with a three-dimensional mesoscale model. *J. Geophys. Res.*, **102** (D12), 13 825–13 834.

Herron, M. M., and C. C. Langway Jr., 1980: Firn densification: An empirical model. *J. Glaciol.*, **25,** 373–385.

Hines, K. M., D. H. Bromwich, and T. R. Parish, 1995: A mesoscale modeling study of the atmospheric circulation at high latitudes. *Mon. Wea. Rev.*, **123,** 1146–1165.

——, ——, and Z. Liu, 1997: Combined global climate model and mesoscale model simulation of Antarctic climate. *J. Geophys. Res.*, **102** (D12), 13 747–13 760.

Jonsson, S., 1992: Local climate and mass balance of a blue-ice area in western Dronning Maud Land, Antarctica. *Z. Gletscherk. Glazialgeol.*, **26,** 11–29.

King, J. C., and W. M. Connolley, 1997: Validation of the surface energy balance over the Antarctic ice sheets in the U.K. Meteorological Office Unified Climate Model. *J. Climate*, **10,** 1273–1287.

——, and J. Turner, 1997: *Antarctic Meteorology and Climatology*. University Press, 409 pp.

Krinner, G., C. Genthon, Z.-X. Li, and P. Le Van, 1997: Studies of the Antarctic climate with a stretched-grid GCM. *J. Geophys. Res.*, **102** (D12), 13 731–13 746.

Louis, J. F., 1979: A parametric model of vertical eddy fluxes in the atmosphere. *Bound.-Layer Meteor.*, **17,** 187–202.

Mellor, M., 1977: Engineering properties of snow. *J. Glaciol.*, **19,** 15–66.

Miller, M. J., T. N. Palmer, and R. Swinbank, 1989: Parameterization and influence of sub-grid scale orography in general circulation and numerical weather prediction models. *Meteor. Atmos. Phys.*, **40,** 84–109.

Morcrette, J.-J., L. Smith, and Y. Fouquart, 1986: Pressure and temperature dependence of the absorption in longwave radiation parameterizations. *Beitr. Phys. Atmos.*, **59,** 455–469.

Nomura, A., 1995: Global sea ice concentration data set for use with the ECMWF re-analysis system. ECMWF Tech. Rep. 76, Reading, United Kingdom, 25 pp.

Roeckner, E., and Coauthors, 1996: The atmospheric general circulation model ECHAM-4: Model description and simulation of present-day climate. Max-Planck-Institut für Meteorologie Rep. 218, 90 pp. [Available from Max Planck Institute for Meteorology, Bundesstrasse 55, D-20146 Hamburg, Germany.]

Sundqvist, H., 1978: A parameterization scheme for non-convective condensation including prediction of cloud water content. *Quart. J. Roy. Meteor. Soc.*, **104,** 677–690.

Tiedtke, M., 1989: A comprehensive mass flux scheme for cumulus parameterization in large-scale models. *Mon. Wea. Rev.*, **117,** 1779–1800.

Turner, J., and Coauthors, 1996: The Antarctic First Regional Observing Study of the Troposphere (FROST) project. *Bull. Amer. Meteor. Soc.*, **77,** 2007–2032.

Tzeng, R.-Y., D. H. Bromwich, T. R. Parish, and B. Chen, 1994: NCAR CCM2 simulation of the modern Antarctic climate. *J. Geophys. Res.*, **99** (D11), 23 131–23 148.

van den Broeke, M. R., 1997: Spatial and temporal variation of sublimation on Antarctica: Results of a high-resolution general circulation model. *J. Geophys. Res.*, **102** (D25), 29 765–29 777.

——, and R. Bintanja, 1995: Summertime atmospheric circulation in the vicinity of a blue ice area in East Queen Maud Land, Antarctica. *Bound.-Layer Meteor.*, **72,** 411–438.

van Lipzig, N. P. M., E. van Meijgaard, and J. Oerlemans, 1998: Evaluation of a regional atmospheric model for January 1993 using in-situ measurements from the Antarctic. *Ann. Glaciol.*, **27,** 507–514.

Walsh, K., and J. L. McGregor, 1996: Simulations of Antarctic climate using a limited area model. *J. Geophys. Res.*, **101,** 19 093–19 108.